Leucine 85 Is an Important Determinant of Divalent Ion Affinity in Rat β-Parvalbumin (Oncomodulin)†

Michael T. Henzl,* Meredith E. Davis, and Anmin Tan

Department of Biochemistry, University of Missouri, Columbia, Missouri 65211

Received August 7, 2008; Revised Manuscript Received October 30, 2008

ABSTRACT: Despite 69% sequence identity with chicken parvalbumin 3 (CPV3), rat β-parvalbumin (β-PV) exhibits a substantially lower Ca^{2+} affinity ($\Delta\Delta G^{o\prime} = 2.0$ kcal/mol). This difference largely reflects the disparate behavior of the respective CD sites. Replacement of the rat β-PV codon with the CPV3 codon at positions 49, 50, and 57−60 produces virtual sequence identity with the CPV3 CD site. However, the resulting protein exhibits a modest (0.5 kcal/mol) improvement in Ca^{2+} affinity, implying that sequence differences beyond the binding site modulate divalent ion binding behavior. The solution structure of Ca^{2+}-free rat β-PV suggested that Leu-85, phenylalanine in CPV3, might be an important determinant. Therefore, the impact of the L85F mutation on divalent ion affinity was examined in rat β-PV, in the variant harboring all six of the aforementioned CD site mutations, and in the intermediate CD site variants. We find that the identity of residue 85, located within the E helix, strongly influences divalent ion affinity in the mammalian β-PV isoform and that its impact is mediated by interactions with residues in the CD site. In the wild-type protein, L85F primarily affects the EF site. By contrast, in the presence of the six CD site mutations, L85F also improves the CD site performance, yielding a protein with Ca^{2+} affinity rivaling that of CPV3 and markedly enhanced Mg^{2+} affinity as well. The impact of L85F on CD site Ca^{2+} affinity is particularly sensitive to the identities of residues 59 and 60. Interestingly, however, significant improvement in CD site Mg^{2+} affinity also requires mutation of additional CD site residues.

Ca^{2+} participates broadly in eukaryotic signal transduction (*1, 2*). EF-hand proteins play a particularly prominent role in Ca^{2+} signaling, functioning as either Ca^{2+}-dependent regulators (e.g., calmodulin) or mobile cytosolic Ca^{2+} buffers (e.g., parvalbumin). These proteins are named for their characteristic divalent ion-binding sites, which consist of a central binding loop flanked by short helices. Recognizing that the spatial orientation of the loop and helices could be mimicked with the fingers of the right hand, Kretsinger coined the term "EF-hand" to describe the motif (*3*−*5*).

Positioned at the approximate vertices of an octahedron, the coordinating ligands are indexed by Cartesian axes (*6*). The $-y$ ligand is an invariant backbone carbonyl; $-z$ is a nearly invariant glutamate, and $-x$ is commonly water. Side chain oxygen atoms supply the remaining ligands. Despite the general similarity of their binding sites, EF-hand proteins exhibit wide variations in divalent ion binding properties.

The crystal structure of carp parvalbumin (PV)[1] established the EF-hand paradigm (*7*). Parvalbumins are small (M_r = 12000), vertebrate-specific proteins (*7*−*9*). The PV family includes α and β sublineages (*10, 11*), distinguished by an isoelectric point (α > 5) and lineage-specific sequence assignments. Mammals express one α and one β isoform (*12*); birds express one α and two β isoforms (*13*).

The PV tertiary structure includes six helical segments, A−F, organized into two domains: the AB domain (residues 1−38) and the CD−EF metal ion-binding domain. The two Ca^{2+}-binding sites are called the CD and EF sites, in reference to the helices flanking the metal ion-binding loop. The CD site spans residues 41−70; the EF site runs from residue 80 to the C-terminus. Although parvalbumins are often viewed as interchangeable high-affinity Ca^{2+} chelators, significant variations in divalent ion affinity have been observed. The β sublineage, in particular, exhibits a spectrum of Ca^{2+} binding behavior, with avian thymic hormone (ATH) and rat β-PV representing the high- and low-affinity extremes, respectively, and CPV3 displaying intermediate affinity (*14, 15*). Elucidation of the physical basis for these differences could advance our understanding of structure−affinity relationships in EF-hand proteins and protein−ligand interactions in general.

Despite 69% sequence identity with CPV3 (Figure 1), rat β-PV exhibits a substantially lower divalent ion affinity ($\Delta\Delta G_{Ca} = 2.0$ kcal/mol). This difference in behavior is largely attributable to the CD site (*13, 15*). The rat β-PV sequence differs from the PV consensus sequence at positions 49, 50, and 57−60. Although replacement of those residues

† This work was supported by NSF Grant MCB0543476 (to M.T.H.).

* To whom correspondence should be addressed. Telephone: (573) 882-7485. Fax: (573) 884-4812. E-mail: henzlm@missouri.edu.

[1] Abbreviations: ATH, avian thymic hormone, an avian β-parvalbumin; CD site, parvalbumin metal ion-binding site flanked by the C and D helical segments; CPV3, chicken parvalbumin 3, an avian β-parvalbumin; DMPC, dimyristoylphosphatidylcholine; DPPC, dipalmitoylphosphatidylcholine; DSC, differential scanning calorimetry; DSPC, distearoylphosphatidylcholine; EDTA, ethylenediaminetetraacetic acid; EF site, parvalbumin metal ion-binding site flanked by the E and F helical segments; EGTA, ethylene glycol bis(β-aminoethyl ether)-*N*,*N*,*N*′,*N*′-tetraacetic acid; Hepes, 4-(2-hydroxyethyl)-1-piperazineethanesulfonic acid; ITC, isothermal titration calorimetry; NaP_i, sodium phosphate; NTA, nitrilotriacetic acid; PV, parvalbumin.

10.1021/bi8014899 CCC: $40.75
Published on Web 11/20/2008

```
        1         10        20        30
RAT β   SITDILSAEDIAAALQECQDPDTFEPQKFFQTSGLS
CPV3    -L-----PS------RD--A--S-S-K----I--M-

           40        50        60        70
RAT β   KMSASQVKDIFRFIDNDQSGYLDGDELKYFLQKFQS
CPV3    -K-S--L-E---IL------FIEE--------R-E-

                 80        90        100
RAT β   DARELTESETKSLMDAADNDGDGKIGADEFQEMVHS
CPV3    G--V--A----TFLA---H--------E------Q-
```

FIGURE 1: Amino acid sequences of rat β-PV (*26*) and CPV3 (*13*). Residue 85 and the CD site residues studied by Henzl and Ndubuka (*16*) are highlighted. The black lines spanning residues 41−70 and 80−108 denote the borders of the CD and EF sites, respectively.

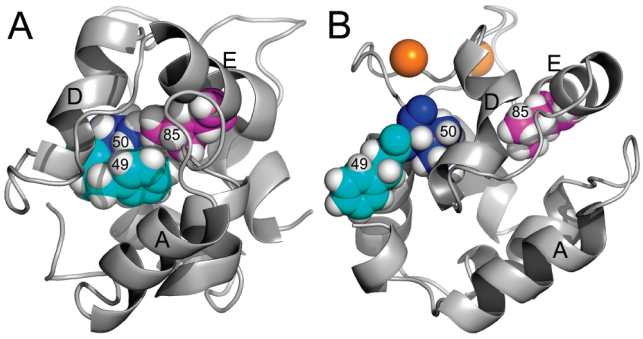

FIGURE 2: Contact between Leu-85 and Phe-49/Ile-50 is abolished by Ca^{2+} binding. The orientations of the F49 (cyan), I50 (blue), and L85 (magenta) side chains are depicted in panel A for the Ca^{2+}-free protein [PDB entry 2NLN (*17*)] and in panel B for the Ca^{2+}-loaded protein [PDB entry 1RRO (*27*)]. Optimal visualization of the side chains in the two structures necessitated a minor reorientation of the molecule. The A, D, and E helices are labeled for reference. This figure and Figure 12 were produced with PyMOL (*28*).

with the corresponding CPV3 residues produces a CD site virtually identical to that in CPV3, the combined mutations have only a minor impact on divalent ion affinity (*16*). Evidently, sequence differences outside the CD site per se must influence its divalent ion binding properties.

The solution structure of Ca^{2+}-free rat β-PV differs substantively from that of the Ca^{2+}-loaded protein (*17*). Ca^{2+} removal provokes reorientation of the C, D, and E helices, reorganization of the hydrophobic core, and remodeling of the AB domain. A major structural alteration involves Phe-49, Ile-50, and Leu-85. F49 and I50 reside at the C-terminal end of the C helix, proximal to the CD site binding loop, which begins at D51. L85 resides in the central region of the E helix. Whereas the side chains of F49 and I50 associate noncovalently with L85 in the Ca^{2+}-free protein, contact is abolished when Ca^{2+} binds (Figure 2). This observation prompted us to examine the consequences of replacing Leu-85 with Phe, the residue present in CPV3. We herein discuss the impact of the L85F mutation in wild-type rat β-PV, in the β variant harboring the aforementioned six substitutions in the CD site, and in select variants harboring subsets of the six CD site mutations. The latter included F49I, F49I/I50L, F49I/I50L/Y57F, F49I/I50L/Y57F/L58I, F49I/I50L/Y57F/L58I/D59E, F49I/I50L/Y57F/L58I/D59E/G60E, and D59E/G60E.

MATERIALS AND METHODS

Materials. Hepes, NaCl, NaH_2PO_4, $CaCl_2 \cdot 2H_2O$, $MgCl_2 \cdot 2H_2O$, $Na_2EDTA \cdot 2H_2O$, EGTA, and NTA were purchased from Fisher Scientific Co. All other common chemicals and reagents were obtained from Fisher or Sigma-Aldrich Fine Chemicals.

Protein Mutagenesis, Expression, and Purification. Mutations were made with the Quik-Change mutagenesis kit (Stratagene). In every case, the fidelity of the resulting sequence was verified by automated DNA sequencing. For brevity, we have adopted the following shorthand notation to designate proteins harboring multiple mutations: 49−50 (F49I/I50L), 49−57 (F49I/I50L/Y57F), 49−58 (F49I/I50L/Y57F/L85I), 49−59 (F49I/I50L/Y57F/L58I/D59E), 49−60 (F49I/I50L/Y57F/L58I/D59E/G60E), and 59−60 (D59E/G60E). The additional presence of the L85F mutation is indicated by /85. For example, 49−50/85 denotes the protein obtained by introducing the L85F mutation into the F49I/I50L variant.

The procedure employed for isolation of the rat β-PV variants has been described previously (*18*). Because the proteins used in this study lack tryptophan, the A_{274}/A_{290} ratio can be used to evaluate homogeneity. The purity of the preparations exceeded 98% in all cases. Concentrations were estimated spectrophotometrically, using extinction coefficients derived from parallel absorbance and interference measurements in a Beckman XL-I analytical ultracentrifuge. The following values (in units of M^{-1} cm^{-1}) were employed: wild-type rat β-PV, 2890; L85F, 3005; F49I, 1610; 49/85, 1660; 49−50, 2970; 49−50/85, 2880; 49−57, 1710; 49−57/85, 1640; 49−58, 1710; 49−58/85, 1680; 49−59, 1650; 49−59/85, 1650; 49−60, 1600; 49−60/85, 1590; 59−60, 3010; 59−60/85, 2980.

Isothermal Titration Calorimetry (ITC). ITC was performed at 25 °C in a MicroCal VP-ITC apparatus. Samples of protein (typically 50−60 μM) were titrated with Ca^{2+} in the presence and absence of competitive chelators (EDTA, EGTA, and NTA) or Mg^{2+} and with Mg^{2+} in the presence and absence of EDTA. A 2 μL preinjection was included at the start of each titration. The heat associated with this addition, invariably low due to diffusion of titrant from the buret during the equilibration period, was neglected during the fitting process.

Following integration of the raw data, using software supplied with the instrument, the resulting composite data set was subjected to simultaneous least-squares minimization, yielding estimates of the binding constants and enthalpies for both Ca^{2+} and Mg^{2+}. The data treatment has been described in detail elsewhere (*14, 19*).

Differential Scanning Calorimetry (DSC). DSC was performed in a modified Nano-DSC instrument (Calorimetry Sciences Corp.) equipped with cylindrical hastalloy cells. Temperature calibration was verified with DMPC, DPPC, and DSPC. The accuracy of the differential power measurements was verified with internally generated electrical calibration pulses.

Samples were dialyzed extensively against 0.15 M NaCl, 0.01 M NaP_i, and 0.005 M EDTA (pH 7.4), which then served as the reference buffer. Sample and reference solutions were degassed briefly under vacuum prior to being loaded. A scan rate of 60 °C/h was employed for all experiments. Each protein included in this study exhibits an exotherm on the cooling scan and an endotherm on rescan, indicating reversible denaturation. A baseline, obtained with sample and reference cells filled with buffer, was subtracted from the

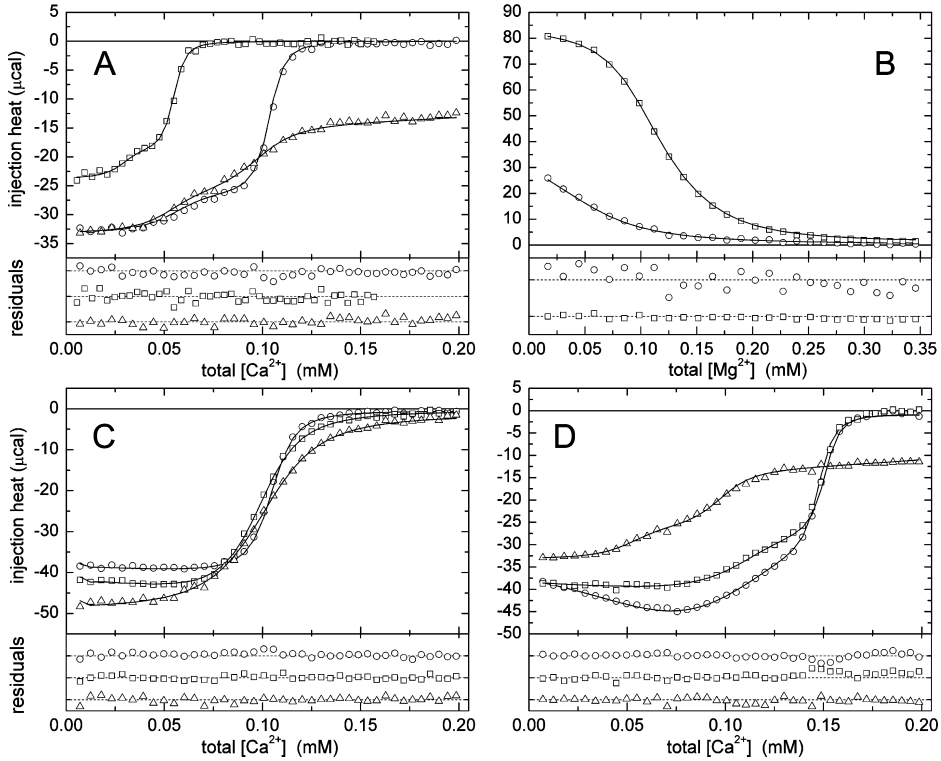

FIGURE 3: Analysis of the divalent ion binding behavior of L85F. Samples were subjected to the battery of titrations described in the text. The integrated data are displayed above, together with the optimal least-squares fit and residuals. Titrant concentrations: 1.10 mM Ca^{2+} and 1.98 mM Mg^{2+}. (A) Ca titrations: 57 μM protein (○), 28 μM protein (□), and 54 μM protein with 0.3 mM NTA (△). (B) Titrations with Mg^{2+}: 57 μM protein (○) and 56 μM protein with 100 μM EDTA (□). (C) Titrations with Ca^{2+} in the presence of Mg^{2+}: 56 μM protein with 1.0 mM Mg^{2+} (○), 54 μM protein with 5.0 mM Mg^{2+} (□), and 56 μM protein with 10.0 mM Mg^{2+} (△). (D) Titrations with Ca^{2+}: 56 μM protein with 60 μM EGTA (○), 56 μM protein with 60 μM EDTA (□), and 56 μM protein with 1.0 mM NTA (△).

protein data prior to analysis. Data collected at several protein concentrations were subjected to global analysis to extract estimates of T_m, ΔH_{cal}, ΔH_{vH}, and ΔC_p, as described previously (*16*). Changes in conformational stability were estimated with the integrated Gibbs−Helmholtz equation:

$$\Delta G(T) = \Delta H_{vH}(T_m)\left(1 - \frac{T}{T_m}\right) + \Delta C_p\left[(T - T_m) - T \ln \frac{T}{T_m}\right] \quad (1)$$

RESULTS

The impact of the L85F mutation was examined in wild-type rat β-PV and in each of the following site-specific variants: F49I, 49−50, 49−57, 49−58, 49−59, 49−60, and 59−60. Four of these proteins have been characterized previously: 49−50, 49−58, 49−59, and 49−60 (*16*).

Characterization of Divalent Ion Binding Behavior. In this study, divalent ion affinity was evaluated by ITC. Each protein was titrated with Ca^{2+}, with Ca^{2+} in the presence of Mg^{2+}, with Ca^{2+} in the presence of competing chelators, and with Mg^{2+} in the absence and presence of EDTA. The resulting data were subjected to simultaneous least-squares minimization to extract estimates of the association constants and binding enthalpies for both Ca^{2+} and Mg^{2+}. Representative global analyses are shown in Figure 3 for the L85F variant of wild-type rat β-PV and in Figure 4 for the 49−60/85 variant.

For all of the proteins examined in this study, the binding data could be accommodated by an independent two-site model, which affords estimates of the microscopic binding constants, k_1 and k_2. In wild-type rat β-PV, the divalent ion affinity of the EF site is decidedly superior to that of the CD site. The Ca^{2+} binding constants for the two sites are 2.3×10^7 and 1.5×10^6 M^{-1}, respectively. The corresponding Mg^{2+} values are 9.2×10^3 and 170 M^{-1}, respectively. We have assumed that the relative affinities are unaltered by the mutations. Thus, k_1 reflects the behavior of the EF site and k_2 the behavior of the CD site.

Examination of the CD Site Variants. Rat β-PV and CPV3 differ at six positions within, or proximal to, the CD binding loop: 49, 50, and 57−60. The divalent ion binding properties of the rat β variants resulting from progressive mutation of these residues are listed in Table 1. Values are also included for the variant harboring only the D59E and G60E substitutions. Panels A and B of Figure 5 display the Ca^{2+} and Mg^{2+} binding constants, respectively, for each of these proteins in bar-graph format. The cross-hatched red bars correspond to the CD site values, and the cross-hatched black bars correspond to the EF site values.

The CD and EF site Ca^{2+} binding constants for wild-type rat β-PV are 1.5×10^6 and 2.3×10^7 M^{-1}, respectively. All of the CD site variants exhibit small improvements in EF site Ca^{2+} affinity (Figure 5A, black cross-hatch). The most significant increase in the EF site binding constant, at 4.9×10^7 M^{-1}, is observed for 49−57. Except for 49−58, all of the variants likewise display minor improvements in CD site Ca^{2+} affinity (Figure 5A, red cross-hatch). 59−60 yielded the most notable increase in the CD site binding constant (3.9×10^6 M^{-1}).

The wild-type Mg^{2+} binding constants for the CD and EF sites are 170 and 9.2×10^3 M^{-1}, respectively. All of the CD site variants display modestly enhanced EF site Mg^{2+}

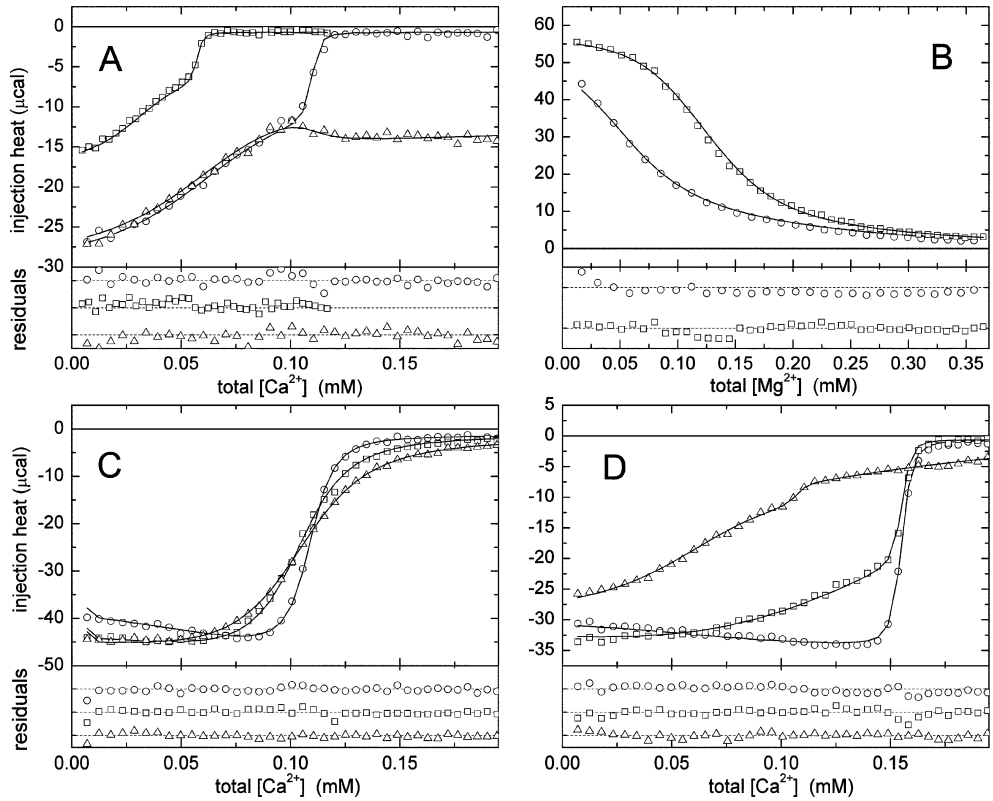

FIGURE 4: Analysis of the divalent ion binding behavior of β 49−60/85. Protein samples were subjected to a suite of titrations, as described in the text. Integrated data, optimal least-squares fit, and residuals are displayed above. Titrant concentrations: 1.10 mM Ca^{2+} and 1.98 mM Mg^{2+}. (A) Titrations with Ca^{2+}: 60 μM protein (○), 30 μM protein (□), and 59 μM protein with 1.0 mM NTA (△). (B) Titrations with Mg^{2+}: 60 μM protein (○) and 59 μM protein with 100 μM EDTA (□). (C) Titrations with Ca^{2+} in the presence of Mg^{2+}: 59 μM protein with 1.0 mM Mg^{2+} (○), 57 μM protein with 5.0 mM Mg^{2+} (□), and 59 μM protein with 10.0 mM Mg^{2+} (△). (D) Titrations with Ca^{2+}: 59 μM protein with 60 μM EGTA (○), 59 μM protein with 60 μM EDTA (□), and 59 μM protein with 100 μM NTA (△).

affinity (Figure 5B, black cross-hatch). The most notable improvement, at 2.16×10^4 M^{-1}, is seen in the 59−60 variant, closely followed by 49−57, 49−58, and 49−59. With respect to CD site Mg^{2+} affinity (Figure 5B, red cross-hatch), F49I and 49−50 actually exhibit smaller Mg^{2+} binding constants. However, the remaining four variants exhibit significant increases. The largest value, at 560 M^{-1}, is observed for 59−60, followed closely by 49−59 and 49−60.

Impact of the L85F Substitution. Figure 5 also illustrates the impact of the L85F substitution on the CD site and EF site binding constants in wild-type rat β-PV and each of the CD site variants. In every case, the mutation substantially improves the EF site affinity for Ca^{2+} (Figure 5A, solid black bars) and Mg^{2+} (Figure 5B, solid black bars). In the presence of L85F, the EF site Ca^{2+} binding constant varies from 7.3×10^7 M^{-1} (L85F) to 1.14×10^8 M^{-1} (49−59/85), as compared to the wild-type value of 2.3×10^7 M^{-1}. The EF site Mg^{2+} binding constant for the L85F variants varies from 3.4×10^4 (49/85) to 5.9×10^4 M^{-1} (49−60/85), as compared to the wild-type value of 9.2×10^3 M^{-1}.

By contrast, the impact of L85F on CD site behavior is more variable. In wild-type rat β-PV, the L85F substitution increases the Ca^{2+} binding constant only from 1.5×10^6 to 2.8×10^6 M^{-1} (Figure 5A, red bars) and the corresponding Mg^{2+} constant actually decreases slightly from 170 to 120 M^{-1} (Figure 5B, red bars). This trend is largely maintained across the series of variants, with minor increases in CD site Ca^{2+} affinity and minor decreases in CD site Mg^{2+} affinity. Only in 49−59, 49−60, and 59−60 does the L85F mutation have a major impact on the CD site binding signature.

In the presence of the rat $\beta \rightarrow$ CPV3 mutations at positions 49, 50, and 57−59, replacement of Leu-85 with Phe increases the CD site Ca^{2+} association constant by a factor of 3.5, from 1.7×10^6 to 6.0×10^6 M^{-1}, and increases the corresponding Mg^{2+} constant by a factor of 2.5, from 5.1×10^2 to 1.3×10^3 M^{-1}.

In the 49−60 background, introduction of L85F produces major increases in Ca^{2+} affinity at both sites. The EF site Ca^{2+} constant improves by a factor of 2.6, from 3.8×10^7 to 1.0×10^8 M^{-1}. The corresponding CD site value increases by a factor of 7.1, from 2.4×10^6 to 1.7×10^7 M^{-1}. These binding constants rival those measured for CPV3. Major improvements are also observed in Mg^{2+} affinity. The EF site constant is increased from 1.6×10^4 to 5.9×10^4 M^{-1}, and the CD site constant is increased from 4.9×10^2 to 2.9×10^3 M^{-1}. The marked improvement in CD site Ca^{2+} affinity is reflected in the binding enthalpy. As noted previously (*16*), the Ca^{2+} titration of 49−60 is distinctly unusual, exhibiting an endothermic second Ca^{2+} binding event [$\Delta H_2 = 2.56$ kcal/mol (Figure 6A)]. Replacement of Leu-85 with phenylalanine in this background restores an exothermic Ca^{2+} binding signature [$\Delta H_2 = -1.02$ kcal/mol (Figure 6B)].

Recognizing that the impact of the L85F mutation on the CD site was most strongly influenced by the identities of residues 59 and 60, we examined the L85F mutation in the variant harboring only the D59E and G60E mutations. The

Table 1: Divalent Ion Binding Properties

	Ca^{2+}				Mg^{2+}			
protein	k_1[a] (M^{-1})	ΔH_1 (kcal/mol)	k_2[a] (M^{-1})	ΔH_2 (kcal/mol)	k_{1M}[a] (M^{-1})	ΔH_{1M} (kcal/mol)	k_{2M}[a] (M^{-1})	ΔH_{2M} (kcal/mol)
rat β-PV[b]	2.30×10^7(2.05, 2.56)	−4.10 (−4.16, −4.06)	1.52×10^6(1.38, 1.70)	−3.46 (−3.52, −3.41)	9.23×10^3(8.93, 9.66)	3.01 (2.97, 3.05)	1.68×10^2(1.58, 1.79)	4.16 (4.00, 4.32)
L85F	7.26×10^7(6.80, 8.18)	−4.31 (−4.44, −4.22)	2.80×10^6(2.50, 3.04)	−3.38 (−3.48, −3.28)	3.90×10^4(3.57, 4.16)	2.04 (1.96, 2.12)	1.17×10^2(1.06, 1.25)	4.94 (4.55, 5.33)
F49I	3.18×10^7(2.90, 3.74)	−4.14 (−4.27, −4.02)	1.93×10^6(1.74, 2.39)	−4.52 (−4.64, −4.39)	1.15×10^4(1.05, 1.29)	3.17 (3.02, 3.35)	1.38×10^2(1.22, 2.25)	4.57 (4.26, 4.98)
F49I/L85F	7.39×10^7(6.69, 8.63)	4.45 (4.60, 4.33)	4.62×10^6(4.09, 5.75)	4.64 (4.77, 4.50)	3.35×10^4(3.07, 3.80)	2.42 (2.26, 2.47)	1.21×10^2(1.04, 1.33)	4.88 (4.60, 5.20)
49−50[c]	3.19×10^7(2.57, 3.80)	3.51 (3.70,3.31)	2.26×10^6(1.90, 2.92)	−3.22 (−3.42, −3.01)	1.34×10^4(1.17, 1.57)	4.22 (3.98, 4.53)	1.46×10^2(1.20, 1.66)	5.42 (5.00, 6.16)
49−50/85	8.32×10^7(7.58, 8.98)	−4.18 (−4.31, −4.10)	4.09×10^6(3.76, 4.66)	−3.92 (−4.00, −3.84)	4.20×10^4(3.88, 4.53)	2.71 (2.59, 2.78)	1.44×10^2(1.33, 1.55)	5.09 (4.88, 5.27)
49−57	4.94×10^7(4.40, 5.78)	−3.57 (−3.68, −3.46)	2.49×10^6(2.26, 3.03)	−3.00 (−3.12, −2.88)	1.72×10^4(1.48, 1.85)	3.24 (3.07, 3.37)	3.68×10^2(3.05, 4.37)	3.92 (3.65, 4.16)
49−57/85	1.00×10^8(0.85, 1.15)	−4.49 (−4.63, −4.36)	4.03×10^6(3.45, 4.79)	−4.00 (−4.12, −3.88)	5.29×10^4(4.44, 5.82)	1.98 (1.88, 2.10)	2.64×10^2(2.26, 3.10)	4.04 (3.79, 4.28)
49−58[c]	4.29×10^7(3.73, 4.68)	−3.78 (−3.89, −3.66)	1.45×10^6(1.31, 1.60)	−3.38 (−3.48, −3.28)	1.79×10^4(1.65, 1.95)	3.39 (3.29, 3.52)	3.34×10^2(2.80, 3.74)	4.26 (4.04, 4.47)
49−58/85	8.42×10^7(7.73, 9.31)	−4.64 (−4.73, −4.50)	2.39×10^6(2.10, 2.60)	−4.06 (−4.14, −3.94)	4.88×10^4(4.57, 5.33)	2.25 (2.16, 2.34)	1.51×10^2(1.36, 1.65)	4.36 (4.12, 4.54)
49−59[c]	4.65×10^7(4.42, 4.89)	−4.92 (−5.02, −4.82)	1.70×10^6(1.64, 1.77)	0.16 (0.12, 0.19)	1.92×10^4(1.82, 2.05)	2.50 (2.38, 2.57)	5.09×10^2(4.68, 5.44)	5.34 (5.13, 5.56)
49−59/85	1.14×10^8(1.03, 1.25)	−5.76 (−5.93, −5.64)	5.97×10^6(5.49, 6.32)	−0.76 (−0.86, −0.68)	4.32×10^4(3.94, 4.93)	1.62 (1.52, 1.76)	1.33×10^3(1.21, 1.57)	4.17 (3.84, 4.38)
49−60[c]	3.76×10^7 (3.46, 4.45)	−3.98 (−4.24, −3.84)	2.43×10^6(2.28, 2.88)	2.56 (2.43, 2.74)	1.60×10^4(1.53, 1.96)	3.34 (2.91, 3.55)	4.91×10^2(4.58, 7.41)	5.78 (5.31, 6.19)
49−60/85	1.01×10^8(0.93, 1.11)	−3.84 (−3.96, −3.76)	1.73×10^7(1.61, 1.82)	−1.02 (−1.07, −0.97)	5.91×10^4(5.56, 6.62)	2.91 (2.82, 3.00)	2.88×10^3(2.62, 3.11)	4.46 (4.32, 4.59)
59−60	4.66×10^7(4.38, 4.94)	−4.03 (−4.12, −3.96)	3.89×10^6(3.69, 4.08)	0.89 (0.83, 0.94)	2.16×10^4(2.04, 2.32)	2.29 (2.20, 2.38)	5.61×10^2(5.22, 6.01)	4.01 (3.85, 4.17)
59−60/85	8.16×10^7(7.43, 8.98)	−3.60 (−3.50, 3.71)	1.15×10^7(1.06, 1.24)	−1.32 (−1.39, −1.26)	5.58×10^4(5.14, 6.14)	2.59 (2.48, 2.69)	4.46×10^2(4.24, 5.09)	5.38 (5.22, 5.60)
CPV3[d]	4.50×10^7(4.31, 4.96)	−5.46 (−5.68, −5.30)	2.43×10^7(2.36, 2.66)	−0.13 (−0.21, −0.04)	4.98×10^4(4.74, 5.79)	1.53 (1.31, 1.62)	2.12×10^4(1.94, 2.38)	1.62 (1.30, 1.76)

[a] Microscopic binding constants, with 68% confidence intervals shown in parentheses. [b] Data from ref *14*. [c] Data from ref *16*. [d] Data from ref *15*.

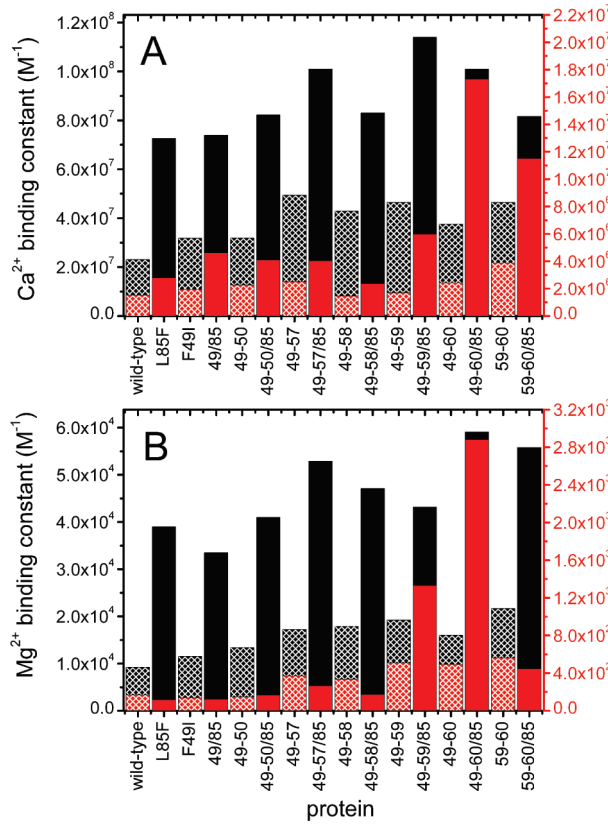

FIGURE 5: Divalent ion binding constants. The binding constants for Ca^{2+} (A) and Mg^{2+} (B) are displayed in bar-graph format. Cross-hatching is used to denote the data for the CD site variants; solid colors are used to denote the corresponding L85F variants. The CD site values are plotted in red and the EF site values in black.

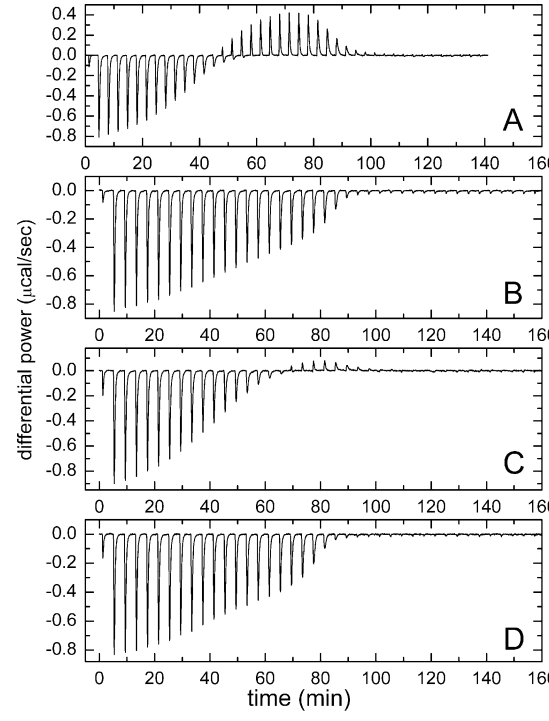

FIGURE 6: Impact of L85F on the ΔH associated with the binding of Ca^{2+} to the 49−60 and 59−60 variants. Representative raw ITC data are presented for 49−60 (A), for 49−60/85 (B), 59−60 (C), and 59−60/85 (D).

results proved to be quite interesting. EF site Ca^{2+} affinity improves from 4.7×10^7 to 8.2×10^7 M^{-1}; EF site Mg^{2+}

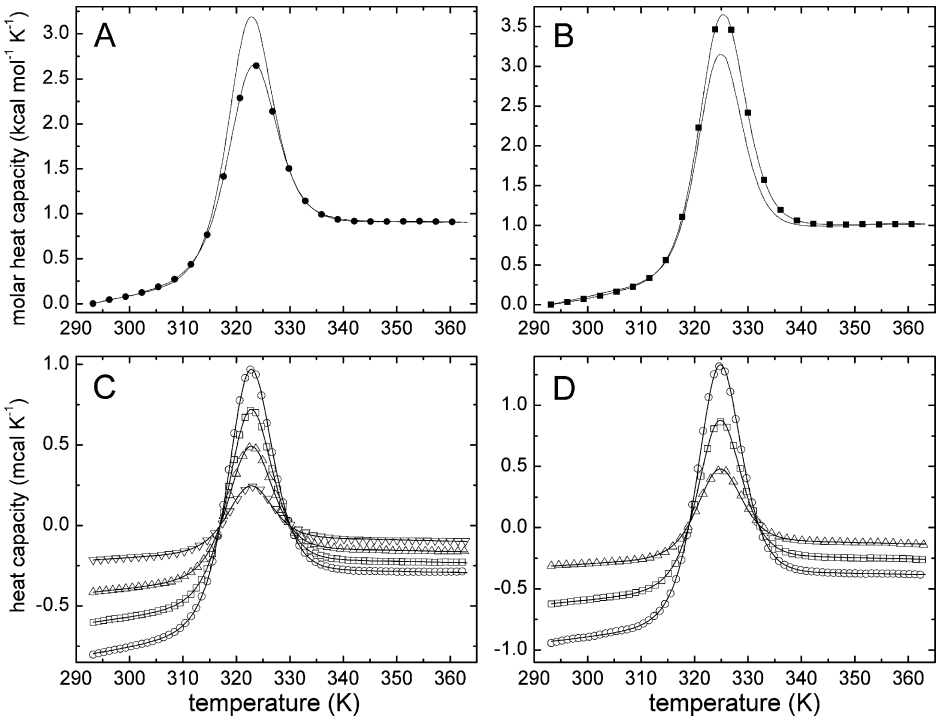

FIGURE 7: Thermal stabilities of L85F and β 49−60/85. These two proteins were analyzed by DSC as described in the text. (A) Molar heat capacities of wild-type rat β-PV (●) and β L85F. (B) Molar heat capacities of β 49−60 (■) and β 49−60/85. (C) Heat capacity data for L85F at 1.75 (▽), 3.50 (△), 5.15 (□), and 6.90 mg/mL (○); $\chi_r^2 = 2.2$. (D) Heat capacity data for β 49−60/85 at 3.10 (△), 5.92 (□), and 9.08 mg/mL (○); $\chi_r^2 = 4.6$. For clarity, only subsets of the data are plotted in panels C and D.

Table 2: Summary of DSC Analyses

protein	T_m[a]	$\Delta\Delta T_m$	ΔH_c	ΔH_{vh}	ΔC_p	$\Delta\Delta G_{conf}$[b]	$\Delta\Delta G_{conf}$[c]
wt rat β-PV	49.3 (49.2, 49.4)	−	72.9 (72.5, 73.1)	67.9 (67.7, 68.2)	1.6 (1.57, 1.63)	−	−
L85F	48.5 (48.4, 48.7)	−0.8	82.3 (82.25, 82.6)	72.9 (72.6, 73.1)	1.98 (1.97, 2.01)	−0.18	−0.03
F49I	50.0 (49.8, 50.2)	0.7	75.2 (75.0, 75.6)	65.2 (64.9, 65.3)	1.74 (1.73, 1.76)	0.14	−0.3
F49I/85	49.2 (49.0, 49.4)	−0.1	71.9 (71.8, 72.3)	68.7 (68.3, 68.8)	1.82 (1.81, 1.86)	−0.02	−0.15
49−50	52.7 (52.6, 52.8)	3.4	86.6 (86.3, 86.9)	69.9 (69.6, 70.1)	1.76 (1.74, 1.80)	0.69	0.20
49−50/85	52.1 (52.0, 52.2)	2.8	80.6 (80.4, 80.9)	70.8 (70.6, 71.1)	1.87 (1.83, 1.88)	0.59	0.12
49−57	52.0 (51.8, 52.1)	2.7	84.8 (84.2, 85.6)	66.0 (65.8, 66.2)	1.94 (1.91, 2.00)	0.53	−0.37
49−57/85	50.9 (50.7, 51.0)	1.6	78.5 (78.2, 78.8)	70.7 (70.4, 70.9)	1.94 (1.91, 1.96)	0.34	−0.02
49−58	51.2 (51.0, 51.3)	1.9	87.0 (86.7, 87.3)	66.0 (65.8, 66.2)	1.98 (1.95, 2.00)	0.38	−0.43
49−58/85	50.8 (50.6, 50.9)	1.5	81.2 (80.9, 81.6)	71.7 (71.3, 71.8)	1.73 (1.72, 1.76)	0.33	0.27
49−59	51.6 (51.4, 51.7)	2.3	86.7 (86.3, 87.0)	68.3 (68.0, 68.5)	1.74 (1.72, 1.77)	0.47	0.03
49−59/85	50.1 (49.9, 50.2)	0.8	79.0 (78.9, 79.3)	72.3 (72.1, 72.4)	1.78 (1.76, 1.80)	0.18	0.22
49−60	51.2 (51.1, 51.4)	1.9	86.5 (86.2, 86.8)	72.2 (72.1, 72.3)	1.70 (1.69, 1.71)	0.41	0.37
49−60/85	50.8 (50.7, 50.9)	1.5	82.4 (82.3, 82.5)	75.8 (75.7, 75.9)	1.72 (1.71, 1.73)	0.34	0.61
59−60	49.6 (49.5, 49.8)	0.3	76.1 (75.4, 76.8)	74.3 (73.7, 74,9)	1.70 (1.63, 1.76)	0.07	0.41
59−60/85	49.0 (48.9, 49.1)	−0.3	78.7 (78.0, 78.9)	76.9 (76.6, 77.4)	1.80 (1.75, 1.84)	−0.07	0.46

[a] Temperatures reported in degrees Celsius, energies in kilocalories per mole, and ΔC_p in kilocalories per mole per kelvin. The 68% confidence intervals are shown in parentheses. [b] Apparent changes in conformational stability at 49.3 °C, the wild-type T_m. Calculated with eq 1. [c] Apparent changes in conformational stability at 25 °C, calculated with eq 1. [d] Data from ref *16*.

affinity improves from 2.2×10^4 to 5.6×10^4 M^{-1}. CD site Ca^{2+} affinity is also significantly improved, from 3.9×10^6 to 1.2×10^7 M^{-1}. However, in distinct contrast to the CD site Ca^{2+} affinity, the L85F mutation actually lowers the Mg^{2+} affinity of the 59−60 CD site, reducing the binding constant from 560 to 450 M^{-1}. As observed for the 49−60 variant, the enthalpy change associated with Ca^{2+} binding at the CD site of 59−60 is endothermic [$\Delta H_2 = 0.89$ kcal/mol (Figure 6C)]. The L85F mutation likewise restores exothermicity to this binding event [$\Delta H_2 = -1.32$ kcal/mol (Figure 6D)].

Impact of the CD Site Mutations on Intrinsic Thermal Stability. The consequences of the L85F substitution in each of the protein settings described above were also examined by DSC. Thermal denaturation was conducted at several protein concentrations, and the resulting data were analyzed globally to extract estimates for T_m, ΔH_{cal}, ΔH_{vH}, and ΔC_p. Representative data and an optimal least-squares fit are shown in Figure 7 for L85F (panels A and C) and 49−60/85 (panels B and D). The optimal DSC parameter values for all 16 relevant proteins are listed in Table 2 and compared in bar-graph format in Figure 8.

The impact of the CD site mutations in the 49−50, 49−58, 49−59, and 49−60 backgrounds has been discussed at length previously (*16*). All four exhibit increased melting temperatures, with ΔT_m values of 3.4, 1.5, 2.3, and 1.9 °C, respectively. All four variants also exhibit substantially larger calorimetric enthalpies of denaturation, with $\Delta\Delta H_{cal}$ values of 13.7, 14.1, 13.8, and 13.6 kcal/mol, respectively. The corresponding $\Delta\Delta H_{vH}$ values are smaller and vary in sign:

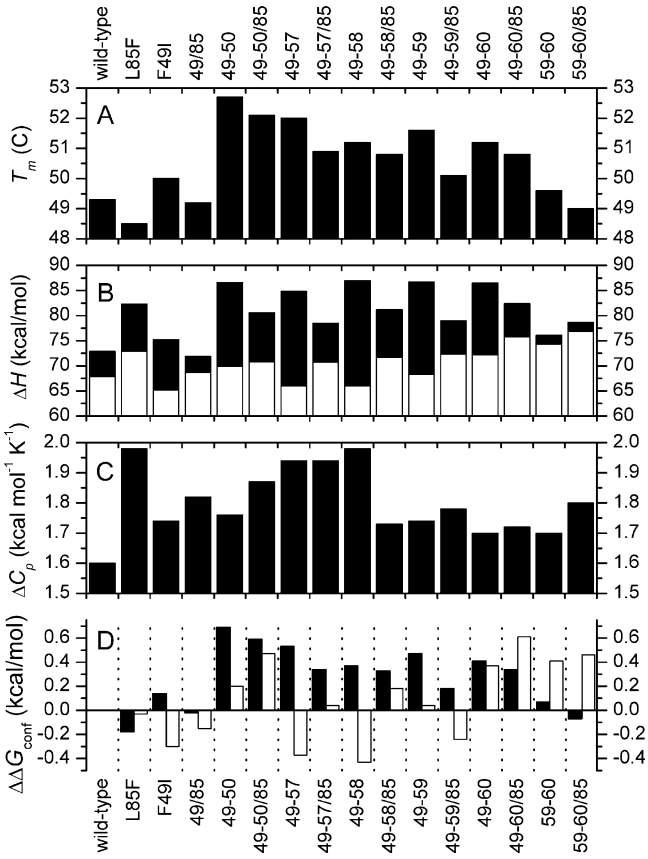

FIGURE 8: Thermal stability parameters associated with each of the proteins examined in this study. (A) Transition temperatures. (B) Calorimetric (black bars) and van't Hoff (white bars) enthalpies of denaturation. (C) Denaturational heat capacity increments. (D) Conformational stabilities, evaluated at 49.3 °C (black bars), the transition temperature for wild-type rat β-PV, and at 25 °C (white bars).

2.0, −1.9, 0.4, and 4.3 kcal/mol, respectively. All four variants exhibit larger ΔC_p values. The increase is greatest for 49−58, 0.38 kcal mol^{-1} K^{-1}, and smaller for the other three, ranging from 0.10 to 0.16 kcal mol^{-1} K^{-1}.

The results for the 49−57 variant are consistent with the previous measurements on the other four proteins, i.e., a significant T_m shift (2.7 °C), a large increase in ΔH_{cal} (11.9 kcal/mol), a small decrease in ΔH_{vH} (−1.9 kcal/mol), and an increase in ΔC_p comparable to that observed for 49−58 (0.34 kcal mol^{-1} K^{-1}). F49I exhibits a smaller ΔT_m, just 0.7 °C; a substantially smaller $\Delta\Delta H_{cal}$, 2.3 kcal/mol; a $\Delta\Delta H_{vH}$ of −2.7 kcal/mol; and a $\Delta\Delta C_p$ of 0.14 kcal mol^{-1} K^{-1}. The 59−60 variant exhibits a ΔT_m of 0.7 °C, a fairly small $\Delta\Delta H_{cal}$, 3.2 kcal/mol; a $\Delta\Delta H_{vH}$ of 6.4 kcal/mol; and a $\Delta\Delta C_p$ of 0.10 kcal mol^{-1} K^{-1}.

When the changes are evaluated at the wild-type T_m, all seven of the CD site variants that were examined exhibit increased stability, relative to wild-type protein, with $\Delta\Delta G_{conf}$ values ranging from 0.07 kcal/mol for 59−60 and 0.14 kcal/mol for F49I to 0.69 kcal/mol for 49−50. The extrapolated stabilities at 25 °C show more variation. Thus, F49I is less stable than wild-type β ($\Delta\Delta G_{conf} = -0.3$), as are 49−57 ($\Delta\Delta G_{conf} = -0.37$) and 49−58 ($\Delta\Delta G_{conf} = -0.43$). However, 49−50 is slightly more stable (0.20 kcal/mol), as are 49−60 (0.37 kcal/mol) and 59−60 (0.41 kcal/mol). The stability of 49−59 is essentially identical to that of the wild-type protein ($\Delta\Delta G_{conf} = 0.03$ kcal/mol).

Impact of the L85F Substitution on Intrinsic Thermal Stability. The L85F mutation produces a reduction in T_m, between 0.4 and 1.1 °C, in all eight proteins. With just two exceptions, L85F decreases the calorimetric enthalpy, with reductions ranging from 3.3 to 7.7 kcal/mol. The exceptions are wild-type rat β-PV and the 59−60 variant, which exhibit increases in ΔH_{cal} of 9.4 and 2.6 kcal/mol, respectively.

In every case, L85F increases the van't Hoff enthalpy. The magnitude of the increase varies from 0.9 kcal/mol (for the 49−50 variant) to 5.7 kcal/mol (for 49−58). Introduction of L85F into the wild-type protein increases the ΔC_p from 1.60 to 1.98 kcal mol^{-1} K^{-1}. Smaller increases are observed for F49I (0.08) and 49−50 (0.11). The mutation significantly reduces ΔC_p when introduced into 49−58 (from 1.98 to 1.73 kcal mol^{-1} K^{-1}). The denaturational heat capacities of the 49−57, 49−59, and 49−60 variants are essentially unchanged by the L85F substitution.

When the impact on stability is assessed at the wild-type T_m, L85F is slightly destabilizing in all of the proteins, with $\Delta\Delta G_{conf}$ values ranging from −0.04 to −0.38 kcal/mol. Due to the differences in ΔH_{vH} and ΔC_p among the variants, the extrapolated changes in conformational stability at 25 °C exhibit greater variation. Thus, F49I, 49−57, 49−58, 49−59, and 49−60 display enhanced stability, with $\Delta\Delta G_{conf}$ values between 0.15 kcal/mol (F49I) and 0.70 kcal/mol (49−58). Wild-type β and the 49−50 variant are slightly destabilized, by 0.03 and 0.08 kcal/mol, respectively.

DISCUSSION

In this discussion, we use the terms "apo" and "Ca^{2+}-free" interchangeably to denote the structures adopted by rat α- and β-PV in the absence of Ca^{2+}. However, the proteins are not, in fact, devoid of metal ions. Under our experimental conditions, the Ca^{2+}-free proteins bind approximately 1.0 and 1.8 equiv of Na^+, respectively (*20*). This monovalent ion binding has a decided stabilizing effect on the proteins (*14, 20, 21*). In fact, Permyakov and co-workers recently observed that two parvalbumins from pike (an α isoform, pI 5.0, and a β isoform, pI 4.2) are largely disordered at very low ionic strengths (*22*).

The CD site in rat β-PV is noteworthy for its attenuated divalent ion affinity. A previous study (*16*) suggested that residues beyond the boundaries of the CD site contribute to this behavior. Specifically, CD site mutations that produce virtual identity with the corresponding site in CPV3 fail to confer a CPV3-like binding signature on the resulting protein.

Although the side chain of L85 dovetails with F49 and I50 in Ca^{2+}-free rat β-PV, the association is abolished when Ca^{2+} binds (Figure 2). This observation suggested that L85 might be a significant determinant of divalent ion affinity. Thus, we have examined the impact of replacing L85 with Phe, the corresponding residue in CPV3, in wild-type rat β and in seven CD site variants exhibiting progressively greater degrees of sequence identity with CPV3.

In the following paragraphs, we first compare the divalent ion binding behavior of the variant proteins to that of wild-type rat β-PV and then explicitly discuss the impact of the L85F mutation in wild-type β and the CD site variants. Because the L85F-provoked changes in divalent ion affinity are context-dependent, we briefly consider the nature of the interactions between residue 85 and the CD site residues, as

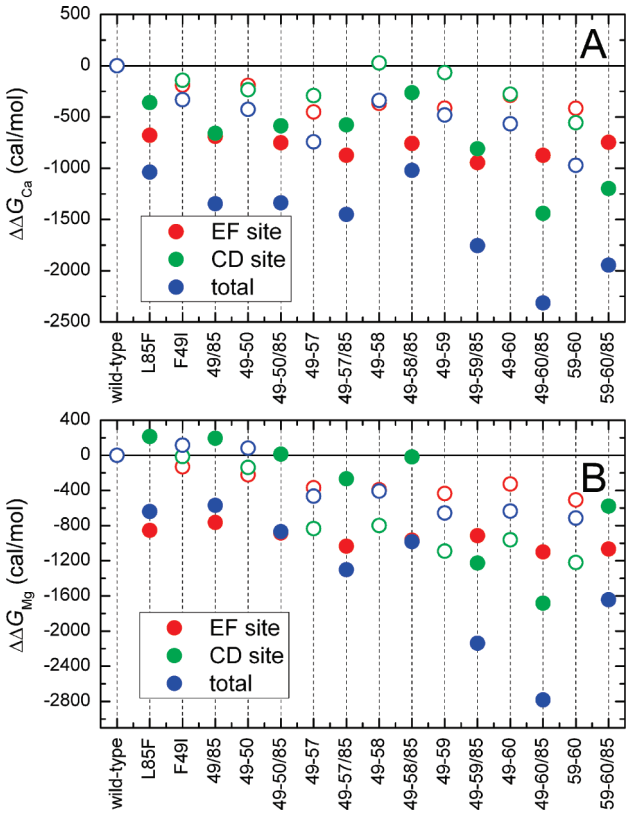

FIGURE 9: Divalent ion binding energetics. The changes in free energy of divalent ion binding, relative to that of wild-type rat β-PV, are displayed for Ca^{2+} (A) and Mg^{2+} (B). Data for the CD site variants are denoted with empty symbols, and data for the corresponding L85F variants are denoted with filled symbols: green for the CD site, red for the EF site, and blue for the overall free energy change.

well as the sign and magnitude of the interaction energies. Following a summary of the impact of the various mutations on the thermal stability of rat β-PV, we close with some speculation about the structural alterations underlying the energetic changes.

Impact of the Mutations on Wild-Type Divalent Ion Affinity. The changes in binding free energy, relative to that of wild-type rat β-PV, that accompany the various mutations are displayed for Ca^{2+} and Mg^{2+} in panels A and B of Figure 9, respectively. The empty symbols represent data for the variants harboring the CD site mutations alone; the filled symbols represent the data for the corresponding L85F variants. Data for the CD site are displayed in green; data for the EF site are displayed in red, and data for their sum are displayed in blue. Table S1 of the Supporting Information summarizes the energetics of divalent ion binding for each of the proteins included in the study.

The Ca^{2+} affinity of rat β-PV (Figure 9A) is relatively insensitive to the CD site mutations. The maximal improvements observed for the CD site (empty green symbols) and the EF site (empty red symbols) were −0.56 and −0.45 kcal/mol, respectively. Mg^{2+} affinity (Figure 9B) is similarly insensitive to the rat $\beta \rightarrow$ CPV3 mutations within the CD site. Improvements at the CD site (empty green symbols) and the EF site (empty red symbols) were limited to −0.71 and −0.51 kcal/mol, respectively.

L85 is located in the E helix. Reflecting this proximity to the EF binding loop, the L85F substitution has a comparable impact on EF site divalent ion affinity in all eight proteins examined. Relative to that of wild-type rat β, the $\Delta\Delta G_{Ca}$ values for the various L85F variants range from −0.68 to −0.94 kcal/mol (Figure 9A, filled red symbols), and the corresponding $\Delta\Delta G_{Mg}$ values (Figure 9B, filled red symbols) range from −0.76 to −1.1 kcal/mol.

Because L85 is distal to the CD site, any influence of L85F on CD site binding properties must arise via interactions with other residues. Not surprisingly, then, the consequences of the mutation on the CD site are more variable. The variants resulting from introducing the L85F mutation into wild-type β, F49I, 49−50, 49−57, and 49−58 exhibit small improvements in CD site Ca^{2+} affinity, with $\Delta\Delta G_{Ca}$ values between −0.28 and −0.52 kcal/mol. In the presence of the $\beta \rightarrow$ CPV3 mutations at positions 49, 50, and 57−59, the $\Delta\Delta G_{Ca}$ associated with the CD site improves by 0.74 kcal/mol, and in the context of all six $\beta \rightarrow$ CPV3 mutations, the improvement increases to 1.16 kcal/mol.

The impact of L85F on the CD site Mg^{2+} affinity exhibits a similar context dependence. The L85F and F49I/85 variants exhibit minor decreases in affinity relative to that of wild-type β; the CD site Mg^{2+} affinities of 49−50/85 and 49−58/85 are essentially unchanged, and 49−57/85 exhibits a small improvement (−0.27 kcal/mol). Only the 49−59/85 and 49−60/85 variants display major increases in Mg^{2+} affinity, with $\Delta\Delta G_{Mg}$ values of −1.22 and −1.68 kcal/mol, respectively. It should be noted that, despite this improvement, the overall Mg^{2+} affinity of 49−60/85 remains nearly 1.1 kcal/mol less favorable than that of CPV3. Clearly, additional sequence differences, besides those discussed herein, must contribute to the attenuation of Mg^{2+} affinity in rat β-PV.

The behavior of 59−60 and 59−60/85 merits comment. In the absence of the mutations at positions 49, 50, 57, and 58, the combined D59E and G60E mutations improve the CD and EF site Ca^{2+} affinities, relative to that of wild-type β, by −0.56 and −0.42 kcal/mol, respectively. The corresponding improvements in Mg^{2+} affinity are −0.71 and −0.51 kcal/mol, respectively. These increases in CD site affinity eclipse those seen with any of the other CD site variants examined. The CD site Ca^{2+} affinity of 59−60/85 is −1.20 kcal/mol more favorable than the wild-type CD site affinity, approaching the improvement seen in 49−60/85 (−1.44 kcal/mol). By contrast, the CD site Mg^{2+} affinity of the 59−60/85 variant is only 0.58 kcal/mol more favorable than that of the wild-type protein, as compared to 1.68 kcal/mol for 49−60/85.

Impact of L85F on Divalent Ion Affinity. The changes in Ca^{2+} and Mg^{2+} binding free energy ($\Delta\Delta G_{Ca}$ and $\Delta\Delta G_{Mg}$, respectively) resulting from the L85F mutation are plotted in panels A and B of Figure 10, respectively, for wild-type rat β and the seven rat β-PV variants. Several interesting trends are evident. For example, the total $\Delta\Delta G_{Ca}$ values (panel A, black bars) are −1.04 and −1.02 kcal/mol when the L85F substitution is performed in wild-type β and F49I, respectively. This quantity decreases progressively in magnitude with the further addition of the I50L (−0.91 kcal/mol), Y57F (−0.71 kcal/mol), and L58I (−0.68 kcal/mol) mutations. The trend is abruptly reversed with the introduction of the D59E (−1.27 kcal/mol) and G60E (−1.75 kcal/mol) mutations. Consistent with this pattern, the impact of L85F on the 59−60 variant ($\Delta\Delta G_{Ca}$ = −0.97 kcal/mol),

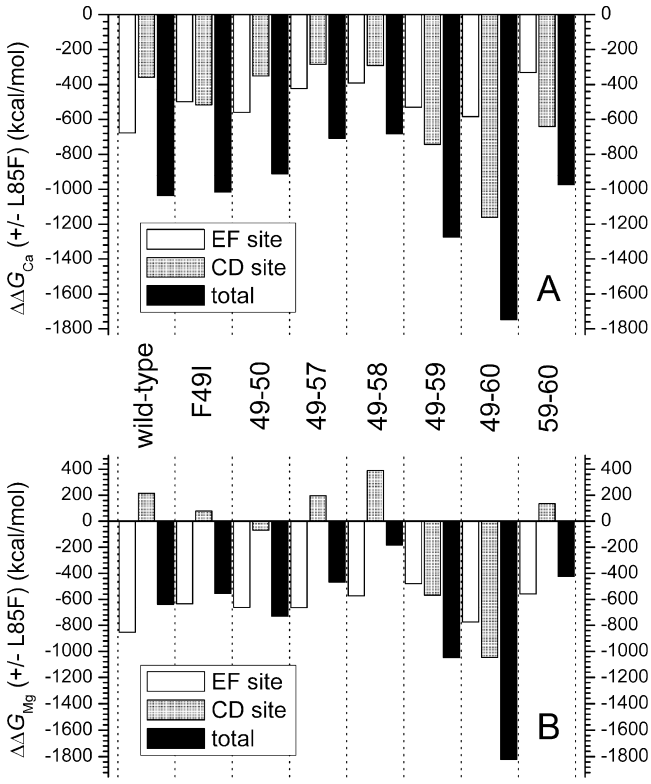

FIGURE 10: Impact of the L85F mutation on the free energy of divalent ion binding. The changes in binding free energy resulting from the L85F substitution in each of the protein settings are displayed for Ca^{2+} (A) and Mg^{2+} (B). The associated EF site changes are displayed in white; the CD site changes are displayed in gray, and their sum is displayed in black.

which of course lacks the mutations at positions 49, 50, 57, and 58, is comparable to that observed in wild-type β.

Although the corresponding data for Mg^{2+} binding display more scatter, the variations in total $\Delta\Delta G_{Mg}$ (Figure 10B, black bars) roughly parallel those observed in $\Delta\Delta G_{Ca}$. Specifically, the magnitudes decrease with the introduction of the Y57F and L58I mutations and then sharply increase with the further mutations at positions 59 and 60.

Inspection of the relative $\Delta\Delta G_{Ca}$ values for the CD and EF sites reveals another interesting pattern. When the L85F mutation is introduced into wild-type rat β, 49−50, 49−57, or 49−58, the improvement in Ca^{2+} affinity at the EF site significantly exceeds that at the CD site. (In the case of F49I, the changes are virtually identical.) By contrast, when the L85F substitution is performed in either 49−59 or 49−60, the improvement in binding free energy associated with the CD site predominates. The 59−60 variant exhibits similar behavior, suggesting that the D59E and G60E mutations strongly modulate the impact of L85F.

The trend in $\Delta\Delta G_{Mg}$ values is qualitatively similar. Whereas L85F mutations in wild-type β, F48I, 49−50, 49−57, or 49−58 produce substantial improvements in affinity at the EF site, they either reduce the CD site affinity or leave it largely unchanged. However, as observed for the $\Delta\Delta G_{Ca}$ values, when the L85F mutation is introduced into either the 49−59 or 49−60 background, the improvement at the CD site becomes dominant. Significantly, the same cannot be said for 59−60. When the L85F substitution is made in this context, the CD site Mg^{2+} affinity is actually decreased ($\Delta\Delta G_{Mg} = 0.13$ kcal/mol), suggesting that elevated

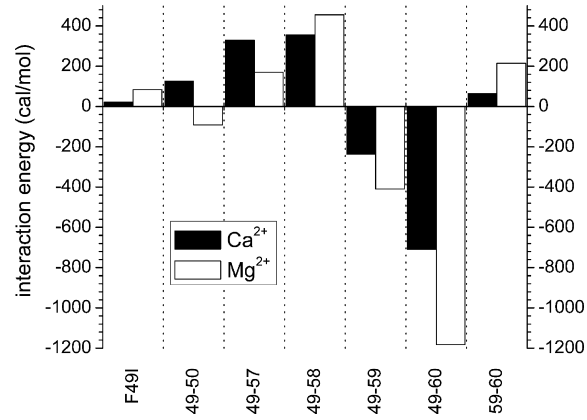

FIGURE 11: Context dependence of the L85F substitution. This overall $\Delta G^{o\prime}$ for divalent ion binding measured for each of the L85F variants was compared to the sum of the $\Delta G^{o\prime}$ values for L85F alone and for the various CD site mutations. The difference is plotted in bar-graph form for Ca^{2+} (black) and Mg^{2+} (white).

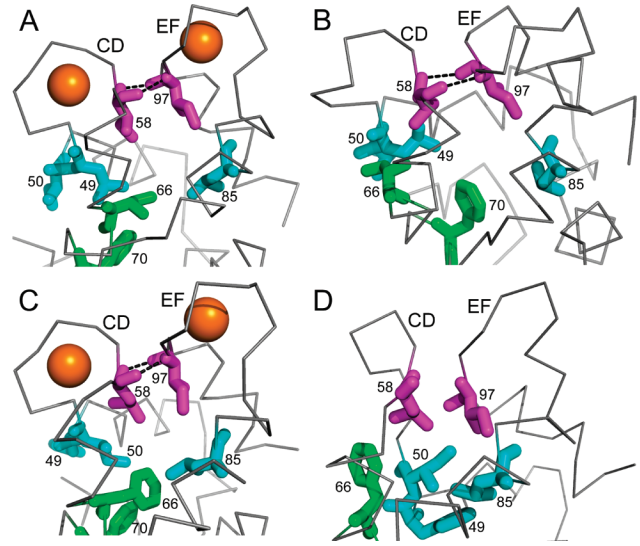

FIGURE 12: Main chain hydrogen bonding between residues 58 and 97 is sensitive to structural rearrangement in the protein interior. Residues 49, 50, and 85, central to the reorganization of the hydrophobic core provoked by Ca^{2+} removal in rat β-PV, are colored cyan. Residues 58 and 97, which form the antiparallel β segment linking the CD and EF loops, are colored magenta. Residues 66 and 70 are colored green. (A) Ca^{2+}-bound rat α-PV. (B) Ca^{2+}-free rat α-PV. Notice that hydrogen bonding between I58 and I97, indicated by the dashed lines, is maintained in the absence of Ca^{2+}. (C) Ca^{2+}-bound rat β-PV. (D) Ca^{2+}-free rat β-PV. Reorientation of residues 49, 50, and 85 evidently abolishes the interloop hydrogen bonding.

Mg^{2+} affinity requires some subset of the other CD site substitutions.

Cooperative Interactions between L85F and the CD Site Mutations. To assess this issue on a semiquantitative basis, we have compared the observed change in binding free energy (relative to that of wild-type β) for each of the L85F variants to the combined $\Delta\Delta G$ values for the (isolated) L85F and relevant CD site mutations. This difference, plotted in Figure 11, is designated an interaction energy because it is indicative of the compatibility of the structural consequences attendant to the L85F mutation and to the sequence adjustments in the CD site.

For example, the overall $\Delta\Delta G_{Ca}$ determined for 49−57/85 is −1.45 kcal/mol. The magnitude of this change is

significantly smaller than the combined changes measured for the 40−57 and L85F variants individually (−1.78 kcal/mol). The positive difference, 0.33 kcal/mol, suggests that the energetic impact of the L85F substitution opposes that resulting from the combined mutations at residues 49, 50, and 57. With just one exception (Mg^{2+} binding to 49−50), qualitatively similar behavior is observed for F49I/85, 49−50/85, 49−57/85, and 49−58/85. In fact, the degree of antagonism increases across this series.

Interestingly, the trend is reversed with the introduction of the D59E mutation. Thus, the interaction energies for Ca^{2+} and Mg^{2+} are both negative for the 49−59/85 variant, indicating a positively cooperative interaction. Inclusion of the G60E mutation further amplifies the favorable interaction between the CD site residues and F85. Significantly, however, the interaction energies for the 59−60/85 variant are slightly positive, suggesting that the synergistic interaction between residue 85 and the CD site residues requires both E59 and E60 and the sequence substitutions at I49, L50, Y57, and L58.

The presence of Asp, rather than Glu, at position 59 is unique to the mammalian β-PV isoform. The side chain of residue 59 contributes the $-x$ ligand to the bound Ca^{2+} in the CD site. When Asp occupies this position, a water molecule serves as the proximal ligand. In this case, the D59 carboxylate is an outer sphere ligand, coordinating the metal ion indirectly via the bound water. By contrast, when Glu resides at $-x$, the longer side chain permits the carboxylate to coordinate the bound Ca^{2+} directly. The potential significance of the Glu → Asp substitution in rat β-PV has been recognized for more than two decades, and it was suggested in the early going that this single sequence difference was largely responsible for the attenuated divalent ion affinity (*23*). That hypothesis was seemingly contradicted, however, by the finding that the D59E mutation has a minimal impact on the Ca^{2+} affinity of rat β-PV (*18*). To further confuse the issue, the reverse mutation (E59D) had a major impact on Ca^{2+} affinity in rat α-PV (*24*). The latter finding led us to propose that the significance of residue 59 as a determinant of parvalbumin divalent ion affinity was strongly context-dependent. This study provides insight into the basis for that context dependence. Although E59 and E60 are indeed necessary for the recovery of divalent ion affinity in rat β, they are not sufficient. Their maximal influence is manifested only in the presence of the L85F substitution and the mutations at positions 49, 50, 57, and 58. This issue is discussed in greater detail below.

Impact of the Mutations on Thermal Stability. The thermal stability parameters for the various proteins examined in this study exhibit some systematic variations. For example, all of the CD site variants exhibit higher T_m and ΔH_{cal} values than wild-type rat β. It is apparent from inspection of Figure 8 that the combination of F49I and I50L has a significantly greater impact on the thermal denaturation behavior than F49I alone. Whereas F49I increases the T_m by 0.7 °C, the increase ranges from 1.9 to 3.4 °C for each of the variants harboring both the F49I and I50L mutations, and whereas F49I increases ΔH_{cal} by 2.3 kcal/mol, the variants having mutations at positions 49 and 50 exhibit $\Delta\Delta H_{cal}$ values between 11.9 kcal/mol (49−57) and 14.1 kcal/mol (49−58). It is tempting to speculate that these differences reflect the noncovalent interaction of both I49 and L50 with residue L85 in the Ca^{2+}-free protein.

Because the effects of the progressive CD site mutations on ΔH_{vH} and ΔC_p are more variable, the extrapolated stabilities at 25 °C exhibit substantial variation. In all cases, however, the observed changes in conformational free energy are modest. The 49−58 variant exhibits the greatest destabilization ($\Delta\Delta G_{conf} = -0.43$ kcal/mol). 49−60 exhibits the largest improvement in stability, 0.37 kcal/mol.

Regardless of the background, the L85F substitution has a qualitatively similar impact on the thermal denaturation parameters. The transition temperature decreases in all cases, with the observed T_m ranging from −0.4 °C (in 49−58 and 49−60) to −1.5 °C (in 49−59). Except for two cases, the calorimetric enthalpies likewise decrease, with $\Delta\Delta H_{cal}$ values ranging from −3.3 kcal/mol (for F49I) to −7.7 kcal/mol (for 49−59). The two exceptions are wild-type β and 59−60, which suggests that the L85F-provoked reduction in ΔH_{cal} also requires (at least) the presence of the F49I mutation.

In contrast to the calorimetric enthalpy, L85F increases the van't Hoff enthalpy of denaturation in each of the variants, with $\Delta\Delta H_{vH}$ values ranging from 0.9 kcal/mol (for 49−50) to 5.7 kcal/mol (for 49−58). Except for the wild-type protein and 49−59, the L85F mutation affords minor increases in conformational free energy at 25 °C. In general, the changes in the stability of the Ca^{2+}-free protein stability are small. However, introduction of the L85F mutation into 49−58 evidently increases the extrapolated ΔG_{conf} at 25 °C by 0.7 kcal/mol.

Potential Structural Basis for the Increased Divalent Ion Affinity of 49−60/85. The solution structure for Ca^{2+}-free rat β-PV was recently reported (*17*). Because the apo and Ca^{2+}-bound proteins exhibit substantial conformational differences, it was suggested that the energetic penalty associated with isomerizing the apoprotein is largely responsible for the attenuated divalent ion affinity displayed by the rat β-PV isoform. According to this hypothesis, parvalbumins displaying more typical divalent ion binding behavior should undergo more limited conformational alteration upon Ca^{2+} binding. Consistent with that prediction, the apo and Ca^{2+}-bound forms of rat α-PV exhibit greater similarity (*25*). The most pronounced structural differences are observed in the extended loops joining the A and B helical elements and the D and E helical elements. The helices per se exhibit only minor changes in placement and orientation.

In wild-type rat β-PV, Ca^{2+} removal provokes a significant rearrangement of the hydrophobic core. For example, the side chains of F66 and F70, tightly packed in the protein interior in the Ca^{2+}-bound state, experience substantial solvent exposure in the apoprotein. By contrast, the side chains of F49, I50, and L85 exhibit the opposite behavior, associating noncovalently within the hydrophobic core in the absence of Ca^{2+}. The conformational change attendant to Ca^{2+} binding breaks the F49/I50−L85 interaction. It also destroys the intimate contact between residues 49 and 50. Although L85 and I50 remain sequestered in the protein interior, F49 undergoes a major reorientation that results in significant solvent exposure.

EF-hand motifs commonly occur in pairs, spatially related by a pseudo-2-fold symmetry axis. In the Ca^{2+}-bound state, the two binding loops are joined noncovalently by a short segment of antiparallel β structure. In parvalbumin, this

fragment of secondary structure is defined by hydrogen bonds between the carbonyl and amide groups of residues 58 and 97. The physical linkage of the CD and EF binding loops provides a structural foundation for energetic linkage between the two sites. The observation that replacement of Leu-85 with Phe strongly perturbs the divalent ion binding behavior of both the EF and CD sites is a reminder that the two sites are part of a cooperative unit.

Presumably, the main chain hydrogen bonding between residues 58 and 97 enables, or encourages, the binding loops to adopt a configuration optimal for interaction between the liganding atoms and the bound divalent metal ions. Interestingly, whereas the fragment of antiparallel β structure between the CD and EF binding loops is evidently retained in Ca^{2+}-free rat α-PV, it is absent in the corresponding form of rat β-PV. Additionally, Ca^{2+} removal provokes a major reorganization of the hydrophobic core in the latter. It is likely, therefore, that the main chain hydrogen bonding between residues 58 and 97 is energetically linked to conformational changes in the hydrophobic core of the protein.

Figure 12 attempts to illustrate this linkage. Panels A and B depict the metal ion-binding domain of rat α-PV in the Ca^{2+}-bound and Ca^{2+}-free states, respectively. The binding loop conformations differ in the two forms, and there has evidently been some local reorientation of residues I49, L50, L66, F70, and L85. However, Ca^{2+} removal does not precipitate a major structural rearrangement. Significantly, the contact between the CD and EF binding loops persists, maintained by the hydrogen bonding between I58 and I97.

Panels C and D depict the corresponding states in the rat β isoform. In the Ca^{2+}-bound protein (panel C), the side chains of F49 and I50 are positioned at the periphery of the hydrophobic core, and F66 and F70 occupy interior positions. In contrast to rat α, Ca^{2+} removal triggers major reorientation of these side chains (panel D). F49 and I50 adopt interior positions to form the aforementioned contact with L85. As a consequence, F66 and F70 are displaced from the hydrophobic core. The rearrangement also perturbs the relative orientations of L58 and I97, with concomitant disruption of the hydrogen bonding between the CD and EF loops.

The combined D59E and G60E mutations significantly increase Ca^{2+} affinity. We suggest that residues 59 and 60 likewise modulate the energetics of the interloop hydrogen bonding, perhaps by influencing the conformation of the polypeptide chain in the vicinity of residue 58. According to this hypothesis, main chain hydrogen bonding between residues 58 and 97 would be facilitated by E59 and E60 and discouraged by D59 and G60. The finding that replacement of E59 with aspartate reduces overall Ca^{2+} affinity in rat α-PV by 1.6 kcal/mol (*24*) is consistent with this idea. Paradoxically, as noted above, the converse mutation (D59E) has a minimal impact ($\Delta\Delta G = -0.1$ kcal/mol) on Ca^{2+} affinity in the rat β isoform (*18, 24*). This observation becomes decidedly less puzzling with the recognition that reorganization of the hydrophobic core in the apoprotein abolishes hydrogen bonding between residues 58 and 97. In the absence of that interaction, the identity of residue 59 should be far less consequential.

The identity of residue 85 is lineage-specific: Leu in members of the α sublineage and Phe in virtually all β isoforms. Thus, the presence of Leu at position 85 in the mammalian β-PV (oncomodulin) is highly unusual. However, the fact that the CD site of rat α-PV retains a high affinity for Ca^{2+} indicates that this sequence identity alone is not sufficient to seriously compromise divalent ion affinity. Evidently, L85 does not confer a low-affinity signature on the CD site unless it occurs in the context of the residue alterations at positions 49, 50, and 58.

We suggest that the F49/I50−L85 interaction is central to establishing and maintaining the atypical conformation of Ca^{2+}-free rat β-PV. Conceivably, replacement of Leu-85 with Phe, in the context of the combined CD site mutations, significantly weakens the 49/50−85 interaction, permitting the apoprotein to adopt a conformation more closely resembling the Ca^{2+}-bound form. If correct, the structure of Ca^{2+}-free 49−60/85 should display interior packing comparable to that of the Ca^{2+}-bound state, and residues 58 and 97 will have assumed the archetypal antiparallel configuration characteristic of paired EF-hand motifs. It will be interesting to learn whether these predictions are borne out and whether the conformation of Ca^{2+}-free 49−60/85 departs significantly from that of the rat β-PV variant harboring only the L85F mutation.

The question of whether the replacement of Phe-85 with Leu in other β-PV isoforms would produce an attenuation of divalent ion affinity comparable to that observed for wild-type rat β-PV arises. In considering this question, we should remember that the rat oncomodulin sequence departs from the PV consensus at positions 49, 50, and 57−60. Furthermore, the six rat β → CPV3 mutations at those positions discussed herein all represent replacements with the PV consensus residue. Given that the L85F mutation has its greatest impact in the context of the 49−60 variant, in which all six positions harbor the PV consensus residue, it is likely that the F85L mutation would strongly perturb the divalent ion binding behavior of other β-PV isoforms.

In summary, the L85F substitution, in concert with the combined CD site mutations, restores CPV3-like Ca^{2+} affinity to rat β-PV. However, the Ca^{2+} affinity of CPV3 is intermediate between that of rat β-PV and more typical PV isoforms (e.g., ATH or rat α-PV). Thus, CPV3 must harbor additional sequence eccentricities which prevent the molecule from displaying a high-affinity divalent ion binding signature. The elucidation of those determinants is a topic for future exploration.

CONCLUSIONS

The low-affinity signature of the CD site in rat β-PV is the product of both local and remote structural determinants. Alone, sequence alterations that produce identity with CPV3 within the CD site fail to confer CPV3-like binding behavior. Similarly, replacement of Leu-85 with phenylalanine in wild-type rat β-PV has little impact on the CD site. However, when combined, the L85F mutation and the CD site modifications act synergistically to imbue the resulting protein with an overall Ca^{2+} affinity exceeding that of CPV3 and markedly improved Mg^{2+} affinity as well. The conformations of apo and Ca^{2+}-bound rat β-PV differ perceptibly. Significantly, the side chains of I49 and L50 associate noncovalently with L85 in the Ca^{2+}-free form. This interaction, which is abolished upon Ca^{2+} binding, may contribute significantly to the stability of the unusual apo conformation.

In the presence of the CD site mutations, the L85F mutation may weaken the contact with residues 49 and 50 sufficiently to permit the apoprotein to adopt a conformation more similar to the Ca^{2+}-loaded state.

SUPPORTING INFORMATION AVAILABLE

Divalent ion binding energetics for each of the variant proteins discussed herein (Table S1). This material is available free of charge via the Internet at http://pubs.acs.org.

REFERENCES

1. Berridge, M. J. (2007) Inositol trisphosphate and calcium oscillations. *Biochem. Soc. Symp. 74*, 1–7.
2. Berridge, M. J., Bootman, M. D., and Roderick, H. L. (2003) Calcium signalling: Dynamics, homeostasis and remodeling. *Nat. Rev. Mol. Cell Biol. 4*, 517–529.
3. Kretsinger, R. H. (1980) Structure and evolution of calcium-modulated proteins. *CRC Crit. Rev. Biochem. 8*, 119–174.
4. Kawasaki, H., and Kretsinger, R. H. (1995) Calcium-binding proteins 1: EF-hands. *Protein Profile 2*, 297–490.
5. Celio, M. R., Pauls, T., and Schwaller, B. (1996) *Guidebook to the Calcium-Binding Proteins*, Oxford University Press, New York.
6. McPhalen, C. A., Strynadka, N. C. J., and James, M. N. G. (1991) Calcium-binding sites in proteins: A structural perspective. *Adv. Protein Chem. 42*, 77–144.
7. Kretsinger, R. H., and Nockolds, C. E. (1973) Carp muscle calcium-binding protein. II. Structure determination and general description. *J. Biol. Chem. 248*, 3313–3326.
8. Heizmann, C. W., and Kagi, U. (1989) Structure and function of parvalbumin. *Adv. Exp. Med. Biol. 255*, 215–222.
9. Pauls, T. L., Cox, J. A., and Berchtold, M. W. (1996) The Ca^{2+}-binding proteins parvalbumin and oncomodulin and their genes: New structural and functional findings. *Biochim. Biophys. Acta 1306*, 39–54.
10. Goodman, M., and Pechere, J. F. (1977) The evolution of muscular parvalbumins investigated by the maximum parsimony method. *J. Mol. Evol. 9*, 131–158.
11. Moncrief, N. D., Kretsinger, R. H., and Goodman, M. (1990) Evolution of EF-hand calcium-modulated proteins. I. Relationships based on amino acid sequences. *J. Mol. Evol. 30*, 522–562.
12. Fohr, U. G., Weber, B. R., Muntener, M., Staudenmann, W., Hughes, G. J., Frutiger, S., Banville, D., Schafer, B. W., and Heizmann, C. W. (1993) Human α and β parvalbumins. Structure and tissue-specific expression. *Eur. J. Biochem. 215*, 719–727.
13. Hapak, R. C., Zhao, H., Boschi, J. M., and Henzl, M. T. (1994) Novel avian thymic parvalbumin displays high degree of sequence homology to oncomodulin. *J. Biol. Chem. 269*, 5288–5296.
14. Henzl, M. T., Larson, J. D., and Agah, S. (2004) Influence of monovalent cation identity on parvalbumin divalent ion-binding properties. *Biochemistry 43*, 2747–2763.
15. Henzl, M., and Agah, S. (2006) Divalent ion-binding properties of the two avian β-parvalbumins. *Proteins 62*, 270–278.
16. Henzl, M. T., and Ndubuka, K. (2007) Low-affinity signature of the rat β-parvalbumin CD site. Evidence for remote determinants. *Biochemistry 46*, 23–35.
17. Henzl, M. T., and Tanner, J. J. (2007) Solution structure of Ca^{2+}-free rat β-parvalbumin (oncomodulin). *Protein Sci. 16*, 1914–1926.
18. Hapak, R. C., Lammers, P. J., Palmisano, W. A., Birnbaum, E. R., and Henzl, M. T. (1989) Site-specific substitution of glutamate for aspartate at position 59 of rat oncomodulin. *J. Biol. Chem. 264*, 18751–18760.
19. Henzl, M. T., Larson, J. D., and Agah, S. (2003) Estimation of parvalbumin Ca^{2+}- and Mg^{2+}-binding constants by global least-squares analysis of isothermal titration calorimetry data. *Anal. Biochem. 319*, 216–233.
20. Henzl, M. T., Larson, J. D., and Agah, S. (2000) Influence of monovalent cations on rat α- and β-parvalbumin stabilities. *Biochemistry 39*, 5859–5867.
21. Henzl, M. T., and Graham, J. S. (1999) Conformational stabilities of the rat α- and β-parvalbumins. *FEBS Lett. 442*, 241–245.
22. Permyakov, S. E., Bakunts, A. G., Denesyuk, A. I., Knyazeva, E. L., Uversky, V. N., and Permyakov, E. A. (2008) Apo-parvalbumin as an intrinsically disordered protein. *Proteins 72*, 822–836.
23. Williams, T. C., Corson, D. C., Sykes, B. D., and MacManus, J. P. (1987) Oncomodulin. ^{1}H NMR and optical stopped-flow spectroscopic studies of its solution conformation and metal-binding properties. *J. Biol. Chem. 262*, 6248–6256.
24. Henzl, M. T., Agah, S., and Larson, J. D. (2004) Rat α- and β-parvalbumins: Comparison of their pentacarboxylate and site-interconversion variants. *Biochemistry 43*, 9307–9319.
25. Henzl, M. T., and Tanner, J. J. (2008) Solution structure of the Ca^{2+}-free rat α-parvalbumin. *Protein Sci. 17*, 431–438.
26. Gillen, M. F., Banville, D., Rutledge, R. G., Narang, S., Seligy, V. L., Whitfield, J. F., and MacManus, J. P. (1987) A complete complementary DNA for the oncodevelopmental calcium-binding protein, oncomodulin. *J. Biol. Chem. 262*, 5308–5312.
27. Ahmed, F. R., Rose, D. R., Evans, S. V., Pippy, M. E., and To, R. (1993) Refinement of recombinant oncomodulin at 1.30 Å resolution. *J. Mol. Biol. 230*, 1216–1224.
28. DeLano, W. L. (2002) The PyMOL molecular graphics system, DeLano Scientific, San Carlos, CA.

BI8014899